Evolution of Pellet Clouds and Cloud Structures in Magnetically Confined Plasmas

L.L. Lengyel, G.G. Zavala, O. Kardaun
and P. Lalousis*

IPP 5/39 January 1990

MAX-PLANCK-INSTITUT FÜR PLASMAPHYSIK

8046 GARCHING BEI MÜNCHEN

MAX-PLANCK-INSTITUT FÜR PLASMAPHYSIK
GARCHING BEI MÜNCHEN

Evolution of Pellet Clouds and Cloud Structures in Magnetically Confined Plasmas

L.L. Lengyel, G.G. Zavala, O. Kardaun
and P. Lalousis*

IPP 5/39 January 1990

*The NET Team, c/o Max-Planck-Institut für Plasmaphysik

EVOLUTION OF PELLET CLOUDS AND CLOUD STRUCTURES IN MAGNETICALLY CONFINED PLASMAS

L.L. LENGYEL, G.G. ZAVALA, O. KARDAUN
Max-Planck-Institut für Plasmaphysik, Euratom Association,
8046 Garching bei München, Federal Republik of Germany
and
P. LALOUSIS
The NET Team, c/o Max-Planck-Institut für Plasmaphysik,
8046 Garching bei München, Federal Republic of Germany,
on leave from Foundation for Research and Technology - Hellas,
Heraklion, Crete, Greece

ABSTRACT

The subject of this study is the spatial and time evolution of initially low-temperature high-density particle clouds in magnetically confined hot plasmas, such as those produced by ablating cryogenic hydrogen pellets in fusion machines. Particular attention is given to such physical processes as heating of the cloud by the energy fluxes carried by incident plasma particles (classical flux-limited energy transport by thermal electrons along the magnetic field lines, anomalous heat conduction across them), gasdynamic expansion with $\vec{j} \times \vec{B}$-produced deceleration in the transverse direction, finite-rate ionization and recombination (collisional and radiative) processes, and magnetic field convection and diffusion.

The results show the existence of a distinct structure in the ablatant cloud surrounding an ablating pellet: a hollow temperature profile coupled to a peaked density profile in the plane normal to the magnetic field direction. The separation distance between the high- and low-temperature and density layers is typically the ionization or confinement radius. Also the flutes developing preferentially at the cloud surface have, at a certain phase of their development, the same wavelength. The temperature and the density variations from the cloud interior to the cloud periphery may exceed two orders of magnitude. The lifetime of this structure is measured on hydrodynamic time scales.

I. INTRODUCTION

An essential problem attracting growing attention in current fusion-oriented plasma physics research is how to replenish particles lost from the plasma volume. The same problem is expected to appear, most likely in a more demanding form, in future magnetic confinement fusion reactors. There are two basic methods currently in use for introducing fresh particles into the plasma volume: gas blow-in (gas puffing) and injection of cryogenic hydrogen isotope pellets into the plasma [1, 2]. Gas blow-in, which is the simplest fuelling method, and which is currently being used in all operational tokamaks, supplies particles to just the outer plasma regions . The relatively low-energy gas stream interacting with the hot plasma particles already becomes ionized and confined to magnetic flux surfaces in the plasma boundary layer. The transport of the injected particles to the plasma core proceeds on a diffusion time scale which, compared with typical pellet injection velocities and associated times, is rather long. Furthermore, the pile-up of the particles in the outer discharge layer may cause increased divertor loading and, at the same time, prevent the formation of peaking density profiles. A further method by which particles are supplied to the plasma from exterior sources is the injection of high-energy neutral particle beams into the plasma, primarily for the purpose of increasing the global plasma energy. This method is also being considered as an auxiliary means of particle fuelling for some specific scenarios. Refuelling by means of low-energy particle beams or by plasmoid ("compact torus") injection are some other alternatives.

The results of numerous experimental and theoretical investigations show that the performance characteristics of present and future tokamaks may be substantially increased by supplying a sufficiently large number of fresh fuel particles direct to the plasma core (see, for example, Alcator-C [3], JET [4], ASDEX [5], TFTR [6], and D-III [7]). In particular, the production of centrally peaked density profiles in tokamak plasmas was found to substantially reduce particle and energy transport in the central plasma region and thus improve the global confinement properties. The density and beta limits observed in pellet-fueled tokamaks were also found to be higher than those in gas-fuelled machines. MHD and sawtooth activities can be notably affected (e.g. suppressed in some cases) by pellet injection. Hence increased attention is being devoted to fuelling by pellet injection. (A detailed review of the state of the art of pellet injection and associated toroidal confinement phenomena may be found in Ref. [8].)

The basic process that determines the effectiveness of pellet fuelling, i.e. the lifetime and penetration depth of cryogenic pellets in hot plasmas, is the pellet erosion or ablation process. This process is of a self-regulating nature: it involves the interaction of the ambient plasma particles with the pellet surface (particle slow-down, energy deposition, surface erosion, and phase transition phenomena), and the build-up of a

buffer layer around the pellet that shields it from the incident particle and energy fluxes. The more effective the shielding, the slower is the ablation process, and vice versa. The physical properties of the ablatant cloud play a decisive role in determining the ablation rate. Hence, from the point of view of predictive (reactor scenario) calculations, there is a strong need for a thorough understanding of all physical phenomena substantially affecting the ablation process.

There have been a number of physical models proposed for describing the pellet ablation process, the best known being the so-called neutral gas shielding ablation model (see Refs. [9, 10, and 11]). This model is based on a one-dimensional spherically symmetric solution of the corresponding hydrodynamic equations. The energy transfer from the undisturbed plasma (the analysis is restricted to thermal electrons as energy carriers) to the cloud surrounding the pellet is calculated by means of stopping length calculations taking elastic and inelastic collisions into account. The violation of the condition of spherical symmetry by the presence of the magnetic field was neglected in these analyses. The effect of the magnetic confinement of the ionized ablatant was estimated in Ref. [12], in which the dynamics of a one-dimensional channel flow (i.e. flow confined to a magnetic flux tube) with a mass source active at the inlet section of the channel was considered. The strength of the mass source, i.e. the ablation rate, was calculated as a function of the local plasma parameters at the channel inlet by means of the Parks-Turnbull formula [10] ("plasma shielding"). The results of this analysis showed the significant effect of the magnetic confinement of the shielding cloud on the ablation rate and thus warranted increased attention to this problem. The neutral gas shielding model was subsequently revised [13] by assuming an ad hoc ionization radius for the ablatant, and that the ionized pellet particles pile up in a channel whose cross-section is defined by this ionization radius. Neither the dimensions nor the parameters of the shielding cloud surrounding the pellet are calculated in this model.

The first estimate of the cloud characteristics was given in Ref. [14] on the basis of zero-dimensional conservation equations (particle, momentum, and energy) by taking finite-rate ionization and magnetic confinement into account. Cloud temperatures and densities of the order of 1 to 3 eV and $10^{24} m^{-3}$ were predicted by this analysis. Parks [15] calculated the distortion of the magnetic field near ablating pellets for the physical domain where the $\vec{j} \times \vec{B}$ force is much smaller than the gasdynamic force grad(p) by neglecting the flow-field interaction. Under these conditions, he found that the magnetic field distortion and the associated magnetic shielding effect are modest. The problem of magnetic shielding was also addressed by Kuteev et al. [16], and by Zavala and Kammash [17]. The question of ablatant expansion and interaction of this high-density partially ionized substance with the magnetic field was recently re-addressed by means of a self-consistent Lagrangian MHD model [18]. The cloud parameters computed in [18b] are in good agreement with measured data reported for PLT [19], TFR [20], TEXT [21], and TFTR [22].

In recent work, Durst [23; see also 21] experimentally investigated the evolution of the ablatant cloud surrounding the pellet. Durst's results show that pellet shielding cannot be viewed as a quasi-equilibrium process: oscillations in the ablation rate are most likely due to oscillations in the pellet shielding, i.e. to the "structures" evolving in the shielding cloud. A notable result of Durst's investigations is the fact that, at least for the range of pellet velocities he investigated (v_{pel} = 700 to 800 m/s), the shape and structure of the ablatant cloud surrounding a moving pellet are not sensitive to the exact location of the pellet in the cloud, as long as it is not about to cross the ionized shell. After crossing the ionization layer, a new "bubble" is blown around the pellet and the cloud evolution is repeated.

Realistic predictions concerning pellet lifetimes, penetration depths, and the required injection velocities for fusion-grade plasmas call for a thorough understanding of the details of those physical processes that determine or substantially affect the lifetime of pellets in hot plasmas. The evolution of the shielding cloud surrounding the pellet is one of these details. In the present work, quantitative information is provided on the variation of the plasmoid state parameters across the shielding cloud surrounding a stationary or slowly moving mass source (e.g. ablating pellet).

II. PHYSICAL MODEL

Let us now briefly describe what is believed to happen when a pellet is injected into a plasma. A cryogenic hydrogen isotope pellet exposed to a hot plasma is heated primarily by the plasma particles, both thermal and non-thermal, incident on the pellet surface. Radiation is believed to affect the pellet much less than the energy fluxes carried by the incident particles. The pellet heating may thus be a surface phenomenon or, in the case of high-energy non-thermal particles, a volume process. In the first case, pellet ablation is equivalent to the sequential removal of molecular layers from the pellet surface. In the second case, pellet heating is usually manifested in an explosion-like mass disintegration. The ablated particles form a dense layer enveloping the pellet. The energy carriers originating from the undisturbed plasma may be partially or totally intercepted by this cloud, and, if this is the case, the pellet "sees" just the cloud layers adjacent to its surface. This low-temperature high-density cloud is heated by the incident plasma particles. In the absence of non-thermal particles, the energy flux carried by the electrons dominates over the flux carried by the ions. As the temperature and the pressure of the cloud increase, the cloud expands: this expansion remains unaffected by the magnetic field (i.e. remains spherically symmetric) as long as the particles remain neutral. During this initial expansion phase, both the total magnetic flux enclosed by the cloud and the energy transfer to the cloud increase proportionally to the cloud dimensions.

At some time instant, the cloud particles begin to become ionized and to interact with the magnetic field, i.e. their radial expansion becomes decelerated and eventually comes to a full stop. For tokamak plasma parameter ranges and particle deposition rates (e.g. ablation rates) of current interest, the stopping radii vary in the mm range (up to a few cm for reactor-grade plasma parameters). The associated stopping times are in the μs range. The expanding partially or fully ionized cloud - referred to hereafter as "plasmoid" - distorts the magnetic field: a transient magnetic cavity may form inside the cloud. Since the gyro-radii of the thermal plasma electrons are usually much smaller than the cloud radius, a reduction of the enclosed average magnetic field is equivalent to a reduction of the energy flux affecting the cloud and the pellet. (The rate of heat input is no longer proportional to the surface area normal to and pierced by the magnetic field lines.) This phenomenon is usually referred to as magnetic shielding.

The radial deceleration and the stopping of the transverse expansion may be followed by a few overdamped compressive oscillations with a characteristic frequency that is defined by the respective Alfvén time: $f^{-1} \approx \tau_A = R_{max}/v_A$, where R_{max} is the maximum cloud radius attained and v_A is the Alfvén velocity based on the cloud density and the applied magnetic field strength [18]. The cause of these oscillations is the periodic interchange of the energies stored in the displaced magnetic field and in the plasmoid. While the dynamic processes associated with the ionization and radial confinement processes are characterized by the relatively short Alfvén time scale (μs range), the subsequent phase of axial expansion is associated with a notably larger hydrodynamic time scale defined by the heat input and gasdynamic expansion rates. The rediffusion of the magnetic field into the ionized cloud occurs on the resistive diffusion time scale, which is of the same order of magnitude as, or larger than, the hydrodynamic time scale (ms range). Because of this relatively slow time variation, this second phase that follows the radial deceleration and confinement processes shall be referred to as the "quasi-steady" or "quasi-equilibrium" phase. During this phase, the plasmoid is "funnelled" into a magnetic flux tube whose radius is given by the plasmoid radius prevailing at the end of the Alfvén oscillations.

The system of equations used for defining the model is analogous to that presented in [18b]: a single-velocity, single-temperature, three-species fluid approximation is used in which the number densities of the species (neutrals, ions, and electrons) are related and defined by means of finite ionization and recombination rates. Allowance is made for the interaction of the conducting cloud with the magnetic field and for the distortion of the applied magnetic field by the expanding plasmoid.

The basic set of magnetohydrodynamic conservation equations used is as follows (the MKS/ISU system of units is used throughout this work):

heavy-particle conservation:

$$\frac{\partial n_h}{\partial t} + \nabla \cdot (n_h \vec{v}) = \dot{n}_s \ , \tag{1}$$

where $n_h = n_a + n_i$;
electron conservation:

$$\frac{\partial n_e}{\partial t} + \nabla \cdot (n_e \vec{v}) = \dot{n}_e \ , \tag{2}$$

momentum conservation:

$$\rho \frac{\partial \vec{v}}{\partial t} + \rho(\vec{v} \cdot \nabla)\vec{v} = -\nabla(p + q_v) + \vec{j} \times \vec{B} + m_s \dot{n}_s (\vec{v}_s - \vec{v}) \ , \tag{3}$$

conservation of total energy:

$$\begin{aligned} &\frac{\partial}{\partial t}\left(\frac{1}{2}\rho v^2 + \frac{p}{\gamma - 1} + \frac{B^2}{2\mu_o}\right) + \nabla \cdot \left[\left(\frac{1}{2}\rho v^2 + \frac{\gamma p}{\gamma - 1}\right)\vec{v}\right] = \\ &\dot{q}_{int} - \nabla \cdot \vec{q} - \nabla \cdot \left(\vec{E} \times \frac{\vec{B}}{\mu_o}\right) + \left(\frac{kT_s}{\gamma - 1} + \frac{1}{2} m_s v_s^2\right)\dot{n}_s . \end{aligned} \tag{4}$$

These equations are supplemented by
Maxwell's equations:

$$\nabla \times \vec{B} = \mu_o \vec{j}, \tag{5}$$

$$\nabla \times \vec{E} = -\frac{\partial \vec{B}}{\partial t}, \tag{6}$$

$$\nabla \cdot \vec{B} = 0; \tag{7}$$

Ohm's law:

$$\vec{j} = \sigma(\vec{E} + \vec{v} \times \vec{B}), \tag{8}$$

a magnetic field diffusion equation (which follows from Maxwell's equations):

$$\frac{\partial \vec{B}}{\partial t} = \nabla \times (\vec{v} \times \vec{B}) + \nabla \cdot (\chi_m \nabla \vec{B}) \ , \tag{9}$$

and an equation of state:

$$p_k = (nkT)_k, \qquad k = e, i, a, s \tag{10}$$

$$\begin{aligned} p &= (n_e + n_i + n_a)kT \\ &= (1 + \alpha) n_h kT. \end{aligned} \tag{11}$$

In the above equations, subscripts e, i, a, h, and s denote, respectively, electrons, ions, neutrals, heavy particles, and particles supplied by the mass source. In the single-velocity approximation used, the momentum conservation equation (3) represents the sum of the momentum balance equations written for the components a, e, and i,

respectively. The quantity q_v appearing in this equation represents artificial viscosity. The particle source strength $\dot{n}_s$ is assumed to be given, whereas $\dot{n}_e$, as will be seen, is calculated on the basis of the plasmoid properties. The cloud density ρ is given by $\rho = n_a m_a + n_i m_i + n_e m_e \simeq n_h m_a$, where m_a is the mass of the neutral atoms considered. Since the present calculations are limited to deuterium, and only dissociative ionization is taken into account, it follows that $D_2 \rightarrow 2D^+ + 2n_e$, and $n_i = n_e$.

The term $\dot{q}_{int}$ appearing in the total energy equation represents internal energy sources: it shall be replaced in our case by a term representing the power per unit volume expended on ionization: $\dot{q}_{int} = -\epsilon_i \dot{n}_e$, ϵ_i being the energy spent on ionization (plus dissociation) of an atom. The magnetic field diffusion coefficient χ_m appearing in eq. (9) is defined by the local value of the electrical conductivity:

$$\chi_m = (\mu_o \sigma)^{-1} , \tag{12}$$

whereas in the calculation of σ both electron-neutral and electron-ion collisions are taken into account:

$$\sigma = \frac{n_e e^2}{m_e \nu_e} , \tag{13}$$

$$\nu_e = \nu_{ea} + \nu_{ei} . \tag{14}$$

The ionization rate equation is of the form

$$\dot{n}_e = n_e n_a \alpha_c - n_e^2 n_i \beta_c + n_a \alpha_\nu - n_e n_i \beta_\nu , \tag{15}$$

where α and β denote the ionization and recombination rates, and the subscripts c and ν collisional and radiative processes, respectively. Detailed equilibrium is assumed and, because of the high collisionality, the equilibrium electron (ion) density is defined in terms of the Saha equation ($n_{eeql} = n_{es}$). In the present work, an effective ionization energy $\epsilon_i \simeq 30\ eV$ is assumed (with allowance for the radiative energy losses associated with the successive excitation and de-excitation processes preceding a single ionization event). Hence, taking advantage of the condition of detailed equilibrium, the ionization rate equation reduces to

$$\dot{n}_e = (\beta_{3b} n_e + \beta_\nu)(n_{es}^2 - n_e^2), \tag{16}$$

where $\beta_{3b} = \beta_c$ is the three-body recombination coefficient [24], and β_ν is taken from Ref. [25]. The collision frequencies ν_{ea} and ν_{ei} are taken from Refs. [15] and [26], respectively.

By subtracting the kinetic and magnetic energy constituents from the total energy, one obtains an equation for the internal energy conservation:

$$\begin{aligned} \frac{\partial}{\partial t}\left(\frac{p}{\gamma - 1}\right) + \nabla \cdot \left(\frac{p\vec{v}}{\gamma - 1}\right) = &- \nabla \cdot \vec{q} - \epsilon_i \dot{n}_e - (p + q_v) \nabla \cdot \vec{v} \\ &+ \left[\frac{kT_s}{\gamma - 1} + m_s (v_s - v)^2\right] \dot{n}_s . \end{aligned} \tag{17}$$

Unlike in all previous spherically symmetric model calculations in which only the heat flux carried by plasma particles confined to and moving along the magnetic field lines was taken into account, in the present model also the transverse conductive heat flux affecting the pellet cloud is accounted for [18]. Indeed, the pellet hose is expanding not in a vacuum, but in a background plasma of rather high temperature. The lateral cloud surface exposed to the surrounding plasma increases in time. The heat fluxes affecting the cloud in the axial and transverse directions are calculated differently: the axial heat flux is defined in terms of the energy flux carried by the thermal electrons along the magnetic field lines, whereas the heat flux in the direction perpendicular to the magnetic field is assumed to be a conductive heat flux defined in terms of an effective thermal conduction across the magnetic field lines. For the first case, a flux-limiting factor of $f_{e_\parallel} = 0.5$ has been assumed, i.e. $q_\parallel = f_{e_\parallel}(\frac{1}{4} n_e v_{e_{th}} E_e)$. Computations performed with this value yielded rather good correspondence with experimentally observed properties [18b]. With regard to the transverse heat flux, an empirical relation consisting of the weighted average of the local thermal conductivities of the neutral gas and electron components, with the local ionization degree as weighting factor, has been used (see [18]). The value of the transverse electron conductivity $\chi_{e_\perp}$ was deduced from experiments aimed at measurement of the heat pulse propagation speeds in tokamak plasmas. Such pulses were produced by, for example, injecting pellets into the plasma [27]. In accordance with Gondhalekar [27], $\chi_{e_\perp} \approx 1 \quad m^2/s$ was used in the present calculations. Axial heat transport by particles other than thermal electrons as well as radial heat transport by particles with sufficiently large gyro-radii (ions) and/or ion conduction have been neglected in these calculations. Admittedly, the combination of the values of $f_{e_\parallel}$ and $\chi_{e_\perp}$, and the neglect of all other energy transport channels is, to a certain extent, arbitrary; only their combined effect was checked against experimental observations ([8], [18b]). Reliable selection of these factors would require series of experiments aimed at determining these quantities.

One will note that the lateral surface of the expanding plasmoid, or at least a major portion of it, is all the time exposed to the background plasma. Owing to axial expansion, this surface continously increases in time. Hence the integrated transverse energy flux may become larger than the axial energy input. In this sense there is no difference between rational and irrational q-surfaces; hence suggestions relating the appearance of striations to the limited length of flux tubes (energy reservoirs) at rational q-surfaces may need to be reconsidered.

To model the radial expansion, ionization, deceleration, and magnetic confinement processes accurately, a 1.5-D multi-cell Lagrangian model has been developed [28] . The radial distributions of the cloud parameters and of the enclosed magnetic field are computed in a self-consistent manner by taking into account the axial (field-aligned) expansion of each Lagrangian cell. This computer model is applied here to various particle deposition scenarios. Note that the questions of pellet heating, pellet erosion, and

pellet disintegration are not considered in the present work. The analysis is limited to the evolution of the cloud formed around the pellet by the ablated pellet particles. The pellet itself is replaced in this model by a mass source (particle source) of given size and given strength. The calculations are performed for a stationary particle source, which, in view of the fact that the average cloud expansion velocities exceed the envisaged pellet flight velocities by a factor of roughly 10, seems to be an admissible approximation.

For the sake of numerical convenience, the expanding and partially ionized particle cloud is subdivided into a discrete number of nested annular volume elements, each annulus representing a Lagrangian cell. The uniform magnetic field applied is assumed to be parallel to the axis of the annulus: $\vec{B} = \hat{z}B(r,t)$. The applied magnetic field is spatially uniform: $\vec{B}(t=0) = \text{const} = \hat{z}B_o$. Since the energy flux due to the plasma particles that affect the cloud is assumed to be identical in the $+\hat{z}$ and $-\hat{z}$ directions, the $z = 0$ plane is assumed to be a symmetry plane and only the $0 \leq z$ domain is considered (i.e. half of the total cloud mass). The initial cloud geometry is given in the form of a regular cylinder $z(k) = \text{const} = z_o, 0 \leq r(\ell) \leq r_p$, where k is the index of a cell (of intrinsic cell properties or cell length) and ℓ is the index of a cell boundary; $r_p = r_{src}$ represents a fictitious source (pellet) radius.

For times $0 \leq t \leq \tau_{src}$ the mass source is turned on, and all Lagrangian cells with inner radii not exceeding the source radius $r_p = r_{src} = \text{const} = R_{c\ell d}(t=0)$ are supplied with cold neutral particles at a rate proportional to their area-coverage ratio: $\dot{N}_{src}(k) = \dot{N}_{src} \cdot a_\perp(k)/A_{\perp src}$, where $\dot{N}_{src}$ is the total mass source strength (equivalent pellet ablation rate), $a_\perp(k)$ is the end surface of the Lagrangian cell covered by (i.e. within the limits of) the source radius, and $A_{\perp src} = \pi r_p^2$ is the total lateral surface of the particle-emitting region. When, in the course of radial expansion, the inner radius of an annular cell becomes larger than r_{src}, the number of particles supplied to this cell is cut to zero. It is assumed that the nested cylindrical annuli retain their initial geometry during the entire cloud expansion, i.e. their boundaries remain nested straight and concentric cylinders. This means, from a mathematical point of view, that the dynamics of the radial expansion is decoupled from that of the axial motion (although, as can be seen from the energy equation, the flow work term used in the calculation of the pressure and/or temperature of a Lagrangian cell takes both the radial and the axial motions into account). Since the primary objective of the present work is to obtain information on the radial structures in ionizing particle clouds expanding in magnetic fields, calculating the axial flow dynamics has the primary purpose of correcting the radial distributions for the effects of axial expansion, and, secondly, of obtaining information on the rate of cloud expansion in the axial direction (length of the structures, etc) as well. Note that the plasmoid expansion in the flux tubes along the magnetic field lines may be viewed as constant-area channel flow with heat addition. The maxima of the respective parallel flow velocities are therefore limited in

this work to the local sonic velocities.

It is of interest to see how the conclusions obtained in the single-cell Lagrangian approximation of [18] become modified in the multi-cell approximation of [28] as used in this work. The major difference between the two approximations is the allowance made for spatially nonuniform ionization (owing to the direct contact between the hot plasma and the outermost plasmoid layer) and the resulting ionization wave propagating toward the plasmoid center (symmetry axis). The radial variations of the ionization state, Lorentz force, magnetic field pressure, etc. taken into account in the present work, affect and modify to some extent the dynamic characteristics of the transition phase and the "quasi-steady" or "quasi-equilibrium" plasmoid properties computed in [18]. Besides its obvious academic interest, the question of radial structures in ablatant clouds has an essential practical application: A pellet injected into a plasma in a direction perpendicular to the magnetic field with a velocity much lower than the average cloud expansion velocity traverses its own shielding cloud. As Durst's study [23, 21] shows, any structures in the medium located ahead of the pellet may affect the local ablation and thus particle deposition rates, the pellet lifetime, and the attainable penetration depths.

The method of solution applied to the above equations is standard: a time- and space-centered explicit finite-difference method to the momentum equations and an implicit method to the radial distributions of the temperature (internal energy) and magnetic field, the latter over the resistive portion of the ablatant cloud. Instantaneous magnetic flux redistribution was assumed for its cold, non-conducting inner core. The interface between the conducting and non-conducting cloud regions moves, of course, inward as the ionization wave captures the inner regions. Details of the Lagrangian formalism used as well as of the numerics involved are given in [28].

The computational model thus defined was applied to a sequence of particle deposition scenarios with a systematic permutation of the four basic input parameters within the ranges indicated:

Ambient plasma (e.g. electron) temperature: $1 < T_{e\infty}\,(keV) < 10$,
Ambient plasma (e.g. electron) density : $10^{18} < n_{e\infty}\,(m^{-3}) < 10^{20}$,
Applied magnetic field strength : $1 < B_o\,(tesla) < 4$, and
Particle deposition rate : $10^{23} < \dot{N}_{src}\,(s^{-1}) < 10^{25}$.

The particle deposition rates selected correspond to ablation rates expected in the central region of large present and next-generation tokamaks.

III. RESULTS OF CALCULATIONS

3.1 Plasmoid evolution: a representative scenario

As a representative or reference case we shall consider a scenario with the following set of initial parameter values:

Background plasma temperature	: T_e^∞	$= 5\ keV$,
Background plasma density (D^+)	: n_e^∞	$= 10^{19}\ m^{-3}$,
Magnetic field strength	: B_o	$= 2.5$ tesla,
Total number of D^o particles deposited in the half-cloud	: N_{htl}	$= 1.6 \times 10^{19}$,
Duration of particle deposition	: τ_{src}	$= 20\ \mu s$,
Temperature of particles deposited	: T_s	$= 15\ ^oK$,
Density of particles deposited	: n_s	$= 6 \times 10^{28}\ m^{-3}$,
Velocity of the source particles	: v_s	$= 0\ m/s$.

The time variation of some representative quantities, such as the total number of heavy particles ($D^o + D^+$) present in the half-cloud, the cloud radius, the average (mass-weighted) cloud temperature and cloud density, and the average ionization degree, are shown in Fig. 1 for the first 25 μs of the cloud evolution. As can be seen, the mass of the cloud continuously increases until $\tau = 20\ \mu s$, and the bulk ionization degree reaches ~ 1.0 at $\tau \approx 16\ \mu s$, remaining at this value for the rest of the mass addition phase. The radius of the cloud reaches a "quasi-steady" value of ~ 4.5 mm in about 1 μs (the ionization time of the outer plasmoid layer). The bulk plasmoid temperature first sharply increases (the kinetic energy increases only slowly because of inertia effects) and, owing to gasdynamic expansion and ionization processes, changes relatively slowly during the subsequent mass addition phase. The bulk plasmoid density decreases exponentially during the first expansion phase but changes relatively slowly for times τ greater than 5 μs. The enclosed total magnetic flux (not shown) rapidly increases as long as the outer cloud layers remain unionized (volume sweeping), and remains practically constant (frozen-in) afterwards. A slow increase of the enclosed magnetic flux can be observed at later times, which is due to magnetic field rediffusion.

The time evolutions of the radial distributions of the cloud pressure, radial Mach number (based on the radial expansion velocity and the local sonic velocity), and local ionization degree are shown in Figs. 2, 3, and 4, respectively, for the duration of the mass addition phase (20 μs). As can be seen, the radial Mach number may reach values greater than unity. Noteworthy is the fact that sonic and supersonic velocities were always found to be limited to the neutral gas expansion domain. As soon as the outer cloud layer becomes ionized, the local expansion velocity drops practically to zero there. All major changes that determine the "quasi-steady" characteristics of the plasmoid are completed during the initial expansion phase associated with the

ionization of the outer cloud layer, and the practically full stop of the radial expansion. Hence a quasi-steady state is associated only with the axial (and not the spherical) expansion phase. The calculated axial velocities (vith the sonic limitation imposed) are in agreement with experimental observations [23].

A time sequence of the radial electron density distribution is shown in Fig. 5. The inward motion of an ionization wave is apparent. The peak of the electron density maximum remains all the time shifted to the left of the locus of the ionization degree maximum, i.e. to the side with lower temperature and higher heavy-particle density. In this example, the peak value of the electron density remains approximately constant ($\sim 10^{24}\ m^{-3}$), while its position is continuously shifted toward the centre of the plasmoid. In the wake of the electron density curve, i.e. on the high-temperature side of the electron density peak, the electron density decreases, both in time and space, because of the axial expansion effects. At the locus of the electron density maximum, the plasmoid is not yet fully ionized.

The length-to-diameter ratios L/D of cloud regions with ionization degrees $\alpha \leq 0.99$ are tabulated in Table 1 for the time at which the maximum radius is reached for a variety of experimental conditions. The length of the neutral cloud fraction is defined here as the mass-weighted average length of all not fully ionized Lagrangian cells. The cloud region in which the particles are not yet fully ionized is the source region of H_α radiation emission. Hence the length-to-diameter ratios shown here can be compared with experimentally observed values. As can be seen, under very different scenario conditions (the number of particles deposited changes by two orders of magnitude, the applied magnetic field strength by a factor of 4) this ratio varies between $\sim$ 3 and $\sim$ 19. For realistic input parameter ranges, the computed values are in agreement with the cloud geometries observed in pellet experiments (see, for example, the CCD and framing camera pictures of Durst [23], or the striations presented by Wurden et al. [29]).

3.2 Field-aligned structures

Owing to the fact that only the outermost plasmoid layer (the outer Lagrangian cell) is in direct contact with the plasma in the radial direction, a conductive heat wave followed by an ionization wave is expected to propagate from the plasmoid periphery toward the symmetry axis. At the same time, since the peripheral layers are being heated at a higher rate than the central ones, they expand in the axial direction, thus causing a rapid density reduction at the plasmoid periphery. There are thus two counteracting physical processes acting at the plasma periphery: the stopping and pile-up of the outward-streaming high-density cloud layers at the ionization radius; the high axial expansion and density reduction rates produced there by the enhanced heat input and the resulting higher temperatures and the associated higher pressure gradients acting along the magnetic field lines. As has been mentioned in the model

description, the axial flow velocity is limited in this analysis to the local sonic velocity a: $w_z = \min(w_z, a)$. Without this limitation, the density reduction due to axial expansion in the peripheral plasmoid layers could be still faster.

The time evolutions of the radial heavy-particle density, temperature, electron density, and magnetic field strength conforming to the representative scenario discussed are reproduced in Figs. 6 to 9 in a continuous manner for the first 3 μs of the cloud expansion time. One can clearly see the growth of the cloud radius up to a time $\simeq 1\ \mu s$, and the transition to a quasi-steady state. As can be seen, the heavy-particle density distribution remains qualitatively "self-similar" during the entire expansion phase (see Fig. 6): it peaks all the time at the centre and decreases monotonically toward the periphery. Hence density reduction due to axial expansion not only balances but also overrides the pile-up of the mass at the ionization radius. This distribution is contrasted by the inverted (hollow) temperature profile (see Fig. 7), the temperature remaining all the time highest at the plasmoid boundary and lowest at the axis of symmetry. (The background plasma temperature is not shown in this figure.) The lifetime and steepness of this hollow temperature profile is determined by the balance between the supply of cold particles to the cloud interior and the heat input rate by thermal diffusion at the cloud periphery. The electron density distribution (see Fig. 8) initially displays a deep hole at the plasmoid axis (for technical reasons, a lower limit was imposed on the electron densities plotted ($10^{16}\ m^{-3}$); the actual electron density approaches zero in this region). This "hole" first expands together with the cold gas volume and then, after the heat flux also penetrates the central plasmoid region, the hollow electron density profile becomes filled up. Obviously, the ionization degree distribution that corresponds to these density and temperature profiles will be similar to the temperature curve with maximum at the plasmoid boundary and minimum at its centre line (see Fig. 4, employing a different time scale). After full ionization is reached, the electron density profile becomes identical to the heavy-particle density profile.

The enclosed magnetic field (Fig. 9) remains spatially uniform and constant in time as long as the cloud remains unionized and expands unaffected by the presence of the magnetic field. Once the outer layer becomes ionized, the enclosed magnetic field is practically frozen-in, and the variation of the interior magnetic field strength is now governed by the motion of the plasma boundary. As can be seen from Fig. 9, the magnetic field strength rapidly decreases in time as the plasmoid radius approaches its maximum value, and then follows the overdamped compressive oscillations of the plasmoid boundary as the transition to the quasi-steady state takes place. At the same time, rediffusion of the magnetic field sets in at the plasmoid boundary. Since the initial plasmoid temperature (electrical conductivity) is rather low, the rediffusion is rapid at the begining and becomes rather slow (measured on the resistive diffusion time scale) at later times.

In summary, the expanding cloud displays a rather characteristic structure during the first phase of its expansion: hollow temperature profile associated with an inward-bound thermal wave (temperature, ionization degree), and an electron density peak that precedes the ionization wave. As time goes on, the temperature distribution becomes more and more filled up at the plasmoid axis and the electron density distribution, once its peak (or the ionization front) reaches the plasmoid axis, becomes identical to the heavy-particle distribution. The heavy-particle distribution remains peaked all the time. The characteristic dimension of the structures thus created in the direction transverse to the magnetic field is given roughly by the ionization radius.

Another phenomenon that may be responsible for field-aligned structures in pellet clouds is the onset of flutes. Indeed, the high-density plasmoid radially decelerating in a magnetically confined low-density plasma is subject to the MHD version of the classical Rayleigh-Taylor instability, i.e. to flute instability. Earlier investigations performed in the single-cell Lagrangian approximation [18a] showed that in a certain expansion phase the wavelength of the flutes expected becomes of the order of the plasmoid radius. In this work, the radial distribution of the local flute wavelengths as well as their time evolution is calculated on the basis of the theory proposed for theta pinches [30]. The ratio of the calculated flute wavelength and the local radius is shown in Fig. 10 for the plasmoid domain in which the local ionization degree exceeds 1/100, and for different time instants. (The input parameters correspond to the representative scenario discussed above.) Note that the cut-off value of the ionization degree (1/100) was selected in a rather arbitrary manner: the theory offered in [30] is, strictly speaking, only applicable to fully ionized plasmas. Hence only the peripheral portions of the curves ($r = R_{cld}$) shown in Fig. 10, which correspond to fully ionized states, can be used with certainty. As can be seen, the wavelengths of flutes always have their maxima at the plasmoid periphery (locus of ion density minimum). This maximum increases in time. At some time instant, which usually lies in the quasi-steady expansion phase, the ratio λ/r reaches the value of π, which is equivalent to an $m = 2$ poloidal disturbance. In this case the field-aligned structure again has a characteristic wavelength defined by the cloud radius, e.g. by the ionization radius. The flutes may thus amplify, during a certain expansion phase, the striated structure associated with the confinement of the ablated particles at the ionization radius. The net effect of flutes may be a sudden and localized ejection of substantial cloud mass fractions (ionized and unionized particles) from the cloud interior. Thus the traces of localized light bursts seen in Fig. 4 of Ref.[23] outside the cloud boundaries may be due to R.-T. instability.

Noteworthy is the radial variation of the thermal energy flux carried by the cloud electrons. The results of calculations show that this quantity increases radially outward and, within the first 10 to 20 μs of the cloud expansion time, it grows also in time at any radial position. For example, in the case of the representative scenario previously

discussed, the ratio $q_{\|cld}/q_{\|e0}$ (subscript "0" denotes here background plasma parameters) reaches, at the end of 10 μs , the value of approximately 0.4 at the cloud centre and approximately 10 at the cloud periphery, i.e. the effective thermal energy flux stored in the peripheral cloud region is in this case an order of magnitude larger than that of the undisturbed plasma. The pellet is most likely (depending upon its flight velocity) going to cross this layer.

3.3 Source strength, magnetic field, and plasma parameter effects

Numerous scenario calculations were made with systematic variation of the four basic input parameters: $\dot{N}_{src}$, n_{e0}, T_{e0}, and B_0, respectively. In each scenario run, the cloud characteristics were monitored at the moment of reaching the maximum cloud radius, and at time instants after the quasi-steady state had been reached (i.e. at 10 μs and 20 μs of the cloud expansion time).

We shall give here a brief description of the effects of the major input parameters on the basic cloud characteristics, as seen from the results of calculations. One should bear in mind that the basic cloud parameter that was found to affect all other quasi-steady characteristics is the stopping or confinement radius. The stopping time associated with the radial confinement of the plasmoid ($\tau(R_{cld} = R_{max})$) is closely related to the ionization time of the outer plasmoid layer and is a complex function of various factors (rate of mass deposition, heat input rate, and magnetic field strength).

Let us now consider the effect of the rate of mass release or particle source strength. The results of calculations show that the cloud radius increases as the number of particles deposited. This is so because it takes longer to ionize a larger number of neutral particles and thus the cloud has a longer time to expand before interaction with the magnetic field begins. The bulk (mass-averaged) cloud temperature of the plasmoid notably decreases whereas the average density increases with increasing mass deposition rate, the latter in spite of the larger cloud cross-sections inherent at higher deposition rates. The bulk ionization degree attained at the moment of radial confinement decreases with increasing source strength. It is noteworthy that the radial expansion of the plasmoid comes to a full stop at relatively low average ionization degree values (0.67 to 0.17 for the cases discussed). Of course, the outer plasmoid layer is already ionized at this time. Figure 11 shows the variation of the maximum cloud radius as a function of the number of particles deposited during the source-on time (all other input data correspond to the representative case discussed above). The radius values at 10 μs and 20 μs expansion time (showing the relatively slow change of the radius during the gasdynamic expansion phase) are also displayed in this figure. Note that pellet penetration depths computed with the help of calculated ionization radii, wich were then fed back into the neutral-gas-plasma-shielding ablation model of Houlberg et al. [13] have shown good correspondence with measured values (see p. 255, Ref.[8]). With regard to the effect of the source strength on the diamagnetic state of the cloud,

the results show that the average magnetic field trapped at the moment of radial confinement decreases with increasing source strength. This is a consequence of the larger initial radial momentum gained in the absence of early ionization: after a frozen-in state has been reached at the plasma periphery, the expanding neutral core continues to push this ionized layer outward, thus further reducing the average magnetic field inside the cloud.

With regard to heat flux (background plasma parameters) and magnetic field effects, the time necessary for ionization of the outer plasmoid shells is a function of the balance between the deposition rate of the cold particles and the heat flux available for heating and ionizing these particles. On the other hand, the confinement radius of the plasmoid layers (and thus the value of all quasi-steady plasmoid parameters) is defined by the balance between the pressure build-up (pressure gradients) and the retarding $\vec{j} \times \vec{B}$ forces, both of which are again functions of the energy input rate (the latter through the electrical conductivity value). In addition, the retarding force is also a function of the magnetic field strength and its distribution as well. The results of calculations show that the "quasi-steady" plasmoid properties are complex functions of all these parameters combined. At low and intermediate plasma temperatures ($T_e^\infty \simeq 5$ keV for the set of representative pellet and plasma parameters considered), the ionization time and hence the vacuum expansion time preceding the moment of interaction with the magnetic field rapidly decrease with increasing incident heat flux. At the same time, the rate of pressure build-up is not sufficient to balance the $\vec{j} \times \vec{B}$ force (except at rather low magnetic field strengths) , and the maximum attainable plasmoid radius continuously decreases with increasing plasma temperature. The stronger the magnetic field, the more pronounced is this effect. At higher energy input rates the pressure build-up is sufficient to prevent further radius reduction or even makes the plasmoid radius grow slightly as the ambient plasma temperature, in spite of the reduced ionization time. The variations of both the maximum attainable and the "quasi-steady" plasmoid radii with the strength of the magnetic field applied are quite pronounced: the stronger the magnetic field the smaller is the stopping radius. The dependence of the average plasmoid density and the bulk plasmoid temperature on the magnetic field strength (i.e. on the magnitude of the stopping radius) is pronounced: the higher the m.f. strength, and thus the smaller the plasmoid radius, the higher is the bulk plasmoid density and the lower is the bulk plasmoid temperature. The plasmoid density, just as the plasmoid radius, is a relatively weak function of the background plasma temperature. More pronounced is the heat flux dependence of the bulk plasmoid temperature. The variation of the volume-averaged cloud density with the background plasma temperature is shown in Fig. 12 for four different magnetic field strengths (again, all other input parameters correspond to the representative case).

With regard to the diamagnetic state of the plasmoid, the plasmoid becomes pronouncedly diamagnetic when subjected to higher heat fluxes (plasma temperatures),

particularly at lower magnetic field strengths. The reason for such behaviour is obvious: higher plasma temperatures means shorter ionization times at the plasma periphery; hence a frozen-in state is reached at an earlier time instant. Furthermore, lower applied magnetic field strengths allow further gasdynamic expansion during the frozen-in state. As a last example, the reduced and volume-averaged magnetic field (averaged "magnetic shielding factor") is shown in Fig. 13 as a function of the background plasma temperature and the magnetic field strength for the time instant of the radial confinement. For further computational results the reader is referred to Ref.[28].

IV. DISCUSSION AND CONCLUSIONS

4.1 Field-aligned structures

Following a short transient spherical expansion phase, the pellet cloud undergoes a quasi-steady linear expansion along the magnetic field lines. This quasi-steady phase is characterized by the presence of field-aligned structures in the cloud state parameter distributions. The separation distance between the field-aligned inhomogeneities evolving during the cloud expansion and ionization processes is related to the only characteristic length inherent in this process: the ionization radius. Gaussian (peaked) density profiles and inverted (hollow) temperature profiles result with function value variation of several orders of magnitude from the plasmoid centre to the plasmoid periphery. Also the structure of the field-aligned flutes that develop at the plasmoid boundary coincides, at some time instant, with an $m = 2$ poloidal disturbance pattern, again with the ionization (confinement) radius as characteristic separation length between them. The lifetime of these structures is measured on hydrodynamic and resistive diffusion time scales.

4.2 Effect of pellet motion

Since the average expansion velocity of the cloud surrounding the pellet is usually much larger than the pellet flight velocity, a pellet crossing its own ablatant cloud is not likely to affect the cloud structure as long as it is not in direct contact with the high-temperature ionized outer shell. However, during passage through the ionization layer, however short this time period may be, the pellet is exposed to heat fluxes that may be considerably higher than those experienced in the interior of the cloud (see Sect. 3.2). Once the pellet is outside the ionization shell, a new low-temperature gas bubble is blown around it and the cloud evolution is expected to repeat itself. Obviously, the ablation rate and the associated cloud expansion dynamics may become strongly modulated by the periodic passages through the high-temperature cloud layers. The alteration of the cloud expansion dynamics and of the ablation rate during the pellet

flight across the ionization shell has not yet been quantitatively clarified. Similarly, also the cloud structures associated with pellet velocities comparable to cloud expansion velocities remain to be investigated.

4.3 Consequences for pellet ablation models

There are no simple or analytical means of quantitatively predicting the physical properties of shielding clouds surrounding ablating pellets. It is possible, of course, by making rather drastic simplifying assumptions regarding the shielding effect, to derive some scaling laws for the pellet penetration depth [8], but no reliable predictions can be made on the basis of these laws. It is also possible to set up empirical or semi-empirical relations for the ablation rate and to validate these models (i.e. to select the values of some free parameters entering these relations) on the basis of experimental results. These models cannot, however, be applied, with a sufficent degree of certainty, to predictive calculations either. Experience shows that validating ablation models and fitting calculated pellet penetration depths, density profiles, etc. to measured ones [31], [32], [33], are rather difficult tasks. Uncertainties and/or scattering in some of the crucial experimental data, such as the actual pellet mass interacting with the plasma, the true pellet velocity and its possible temporal variation, the electron temperature profile immediately prior to pellet injection, etc., make validation rather difficult. Ablation rates and pellet penetration depths observed in different tokamaks were reproduced by means of different ablation models, which, however, are not supposed to be machine-specific. The experimental observations of Durst et al. [21] and others, as well as the results of the present and previous calculations [18], indicate that ablation is an inherently transient process determined on the whole by the evolution of the shielding cloud around it and by the modulation of the cloud characteristics (in space and time) by the presence of the magnetic field (the magnetic confinement of the ionized fraction of the cloud). Hence an ablation model that is predestined for predictive pellet penetration calculations in fusion-grade plasmas should take these aspects into account. Besides, the development of such a model should be accompanied by experiments with accurate measurements of all essential data concerning not only the pellet-plasma interaction but also the shielding cloud evolution processes. The shielding cloud models, too, need verification or validation.

ACKNOWLEDGEMENT

Part of this analysis was carried out in the framework of a doctoral thesis. One of the authors (G.Z.) wishes to expess his sincere appreciation to Max-Planck-Institut für Plasmaphysik at Garching for providing him with financial support and guidance for the duration of his study.

REFERENCES

(1) CHANG,C.T., JORGENSEN,L.W., NIELSEN,P., and LENGYEL,L.L., Nucl. Fusion **20** (1980) 859.

(2) MILORA,S.L., J. Fusion Energy **1** (1981) 15.

(3) GREENWALD,M., GWINN,D., MILORA,S.L., PARKER,J., PARKER,R., et al., Phys. Rev. Lett. **53** (1984) 352.

(4) SCHMIDT,G.L. and the JET-Team, Plasma Phys. and Contr. Nucl. Fus. Res., Proc. of the 12th IAEA Conf., Nice, 1988, Vol. **1**, 215.

(5) KAUFMANN,M., BEHRINGER,K., FUSSMANN,G., GRUBER,O., LACKNER,K., et al., Plasma Phys. and Contr. Nucl. Fus. Res., Proc. of the 12th IAEA Conf., Nice, 1988, Vol. **1**, 229.

(6) ZARNSTORF,M.C., ARUNASALEM,V., BARNES,C.W., BELL,M.G., et al., Plasma Phys. and Contr. Nucl. Fus. Res., Proc. of the 12th IEAE Conf., Nice, 1988, Vol. **1**, 183.

(7) SCHISSEL,D.P., "Pellet Injection Experiments on DOUBLET-III", Presentation at the International Pellet Workshop, La Jolla, Calif. Oct./Nov. 1985

(8) Proc. IAEA Techn. Comm. Meeting on Pellet Injection and Toroidal Confinement,Gut Ising, FRG, 1988, IAEA-TECDOC-534, Vienna, 1989; or see LENGYEL, L.L., Conference Report, Nuc. Fusion **29** (1989) 325.

(9) PARKS,P.B., TURNBULL,R.J., and FOSTER,C.A., Nucl. Fusion **17** (1977) 539.

(10) PARKS,P.B. and TURNBULL,R.J., Phys. Fluids **21** (1978) 1735.

(11) MILORA,S.L. and FOSTER,C.A., IEEE Trans. Plasma Sci. **6** (1978) 578.

(12) KAUFMANN,M., LACKNER,K., LENGYEL,L.L., and SCHNEIDER,W., Nucl. Fusion **26** (1986) 171.

(13) HOULBERG,W.A., MILORA,S.L., and ATTENBERGER,S.E., Nucl. Fusion **28** (1988) 595.

(14) LENGYEL,L.L., Phys. Fluids **21** (1978) 1945.

(15) PARKS,P.B., Nucl. Fusion **20** (1980) 311.

(16) KUTEEV,B.V., UMOV,A.P., and TSENDIN,L.D., Sov. J. Plasma Phys. **11** (1985) 236.

(17) ZAVALA,G., and KAMMASH,T., Fus. Technology, **6** (1984) 30, see also: Bull. Am. Phys. Soc. **28** (1983) 1151.

(18) LENGYEL,L.L., (a) Phys. Fluids **31** (1988) 1577; (b) Nucl. Fusion **29** (1989) 37.

(19) McNEIL,D.H., GREENE,G.J., and SHURESKO,D.D., Phys. Rev. Lett. **55** (1985) 1398.

(20) TFR GROUP, Europhys. Lett. **2** (1986) 267.

(21) DURST,R.D., ROWAN,W.L., and COLLINS,R.A., Bull. Am. Phys. Soc. **32** (1987) 1841.

(22) McNEIL,D.H., OWENS,D.K., and SCHMIDT,G.L., Bull. Am. Phys. Soc. **32** (1987) 1926.

(23) DURST,R.D., ROWAN,W.L.,et al., Nucl. Fusion **30** (1990) 3; see also DURST,R.D., Ph. D. Thesis, The University of Texas, Austin, Texas, 1988.

(24) HINNOV,E. and HIRSCHBERG,J.G., Phys. Rev. **125** (1962) 795.

(25) ZEL'DOVICH,Y.B. and RAISER,Y.P., Physics of Shock Waves and High-Temperature Hydrodynamic Phenomena. Academic Press, N.Y., 1967.

(26) SPITZER, L., Physics of Fully Ionized Gases, Interscience Publishers Inc., N.Y.. 1956.

(27) GONDHALEKAR,A., CHEETHAM,A.D, HAAS,J.C.M., JARVIS,O.N., MORGAN,P.D. et al., in Proc. IAEA Techn. Comm. Meeting on Pellet Ablation and Toroidal Confinement, Gut Ising, FRG, 1988, IAE-TECDOC-534, Vienna 1989, p.113.

(28) ZAVALA,G., "Evolution of High-Density Particle Clouds in Magnetically Confined Plasmas", Ph.D. Thesis, The University of Michigan, Ann Arbor, Mich., Dec. 1989; see also IPP Rept. 5/33, 1990 (in preparation).

(29) WURDEN,G.A., BÜCHL,K., CAYTON,T.E., LANG,R.S., at al., Proc. 16th Europ. Cof. on Contr. Fus. and Pl. Phys., Venice, **13 B** (1989) Pt. IV, 1561.

(30) KEILHACKER,M., KORNHERR,M., NIEDERMEIER,H., SÖLDNER,F., and STEUER,K.H., Phys. Rev. Lett. **32**, 1044 (1974).

(31) WATKINS,M.L., HOULBERG,W.A.,CHEETHAM,A.D., et al., in Proc. 14th Europ. Cof. on Contr. Fus. and Pl. Phys., Madrid, 1987, Vol.**11D** Pt. I, 201.

(32) GOUGE,M.J. HOULBERG,W.A., MILORA,S.L., and SHURESKO,D.D., Bull. Am. Phys. Soc. **32** (1987) 1840.

(33) LENGYEL,L.L., BŨCHL,K., and SANDMANN,W.,
in Proc. 16th Europ. Cof. on Contr. Fus. and Pl. Phys., Venice, 1989, Vol.13B Pt. I, 179.

Table 1. Length-to-diameter ratio L/D of the not fully ionized region (mass-weighted average length of cells with $\alpha \leq 0.99$, which is the region of possible H_α radiation emission, divided by the cloud diameter) at the moment when the maximum cloud radius is reached for different ablation scenarios.

a) The total number of particles N_{hlf} deposited within $\tau_{src} = 20\mu s$ is varied*:

N_{hlf}	L/D
2.0×10^{18}	19.3
5.5×10^{18}	13.7
1.6×10^{19}	9.3
4.4×10^{19}	4.8
1.3×10^{20}	2.9

b) The applied magnetic field strength B_o and plasma temperature are varied*:

B(tesla)	L/D (5 keV)	L/D (7 keV)
1.0	2.8	2.6
2.0	7.3	7.7
3.0	10.7	11.0
4.0	12.0	13.6

* All other conditions are identical to those specified for the "representative case".

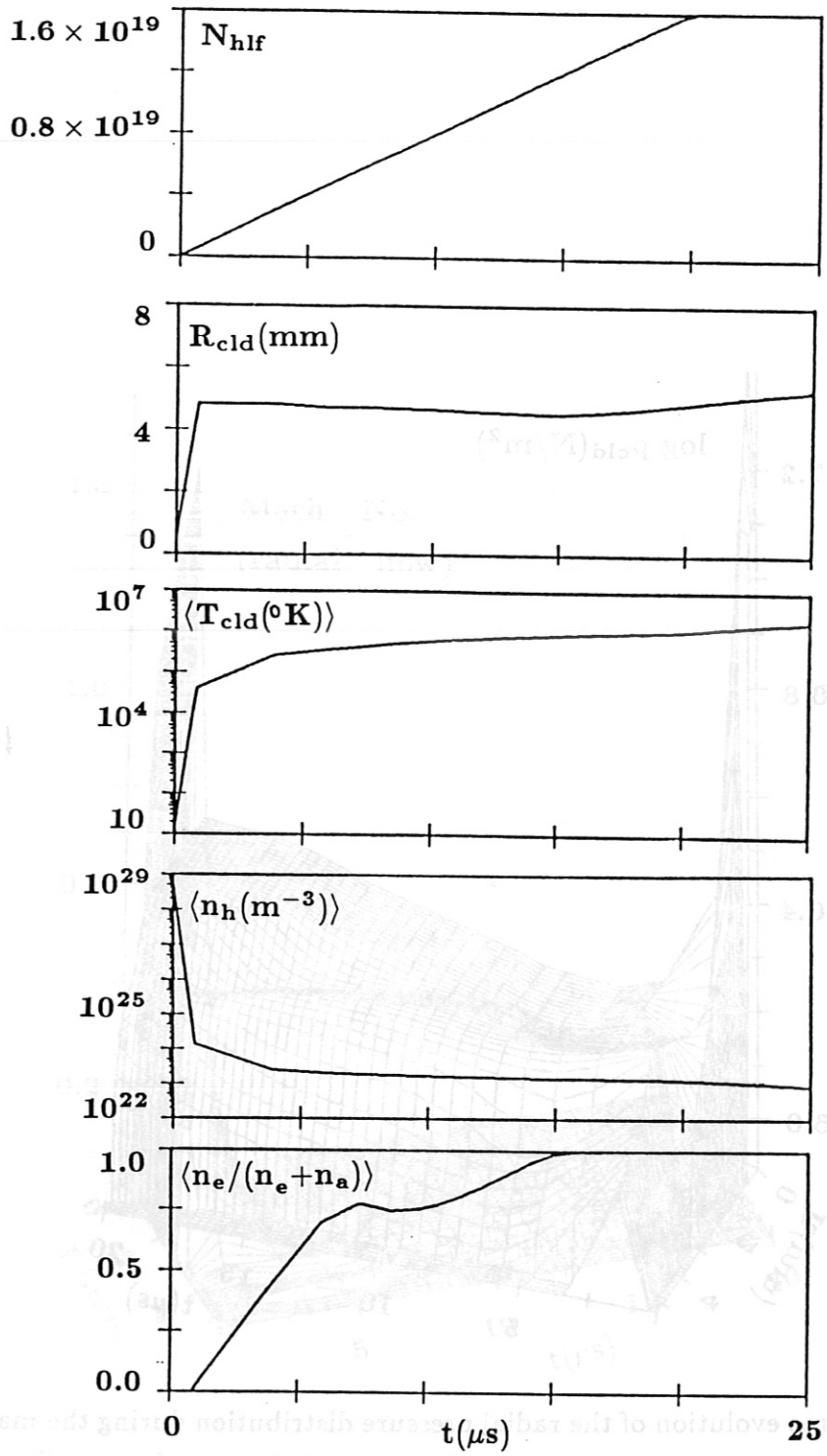

Figure 1: Time variation of representative cloud parameters for the first 25 μs.

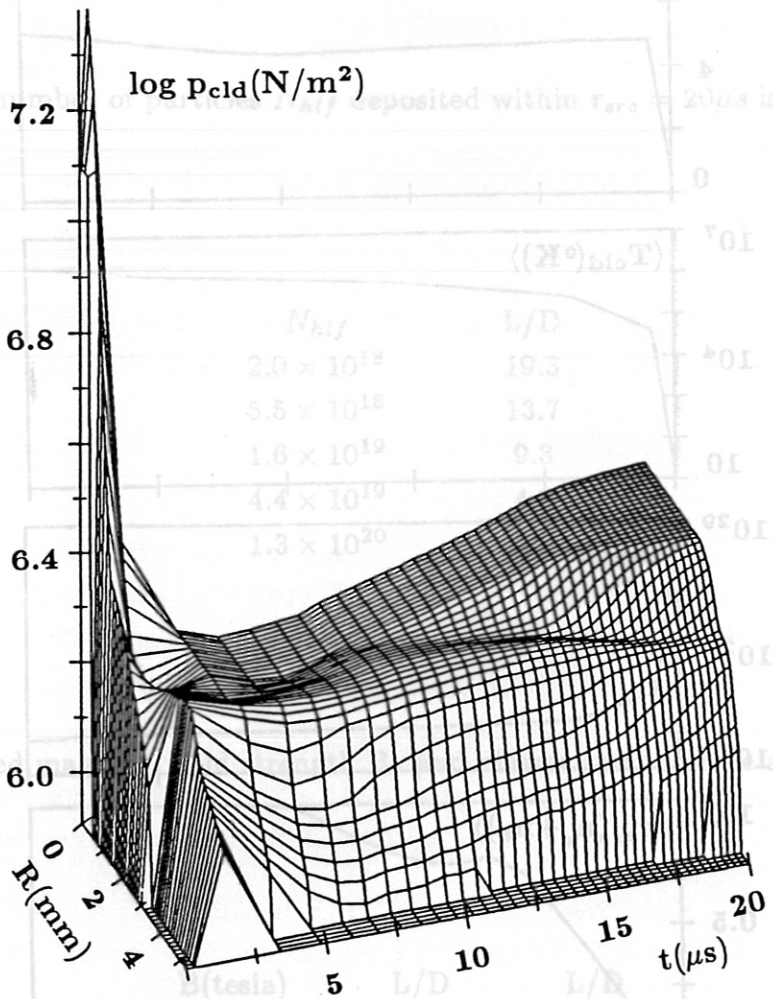

Figure 2: Time evolution of the radial pressure distribution during the mass addition phase.

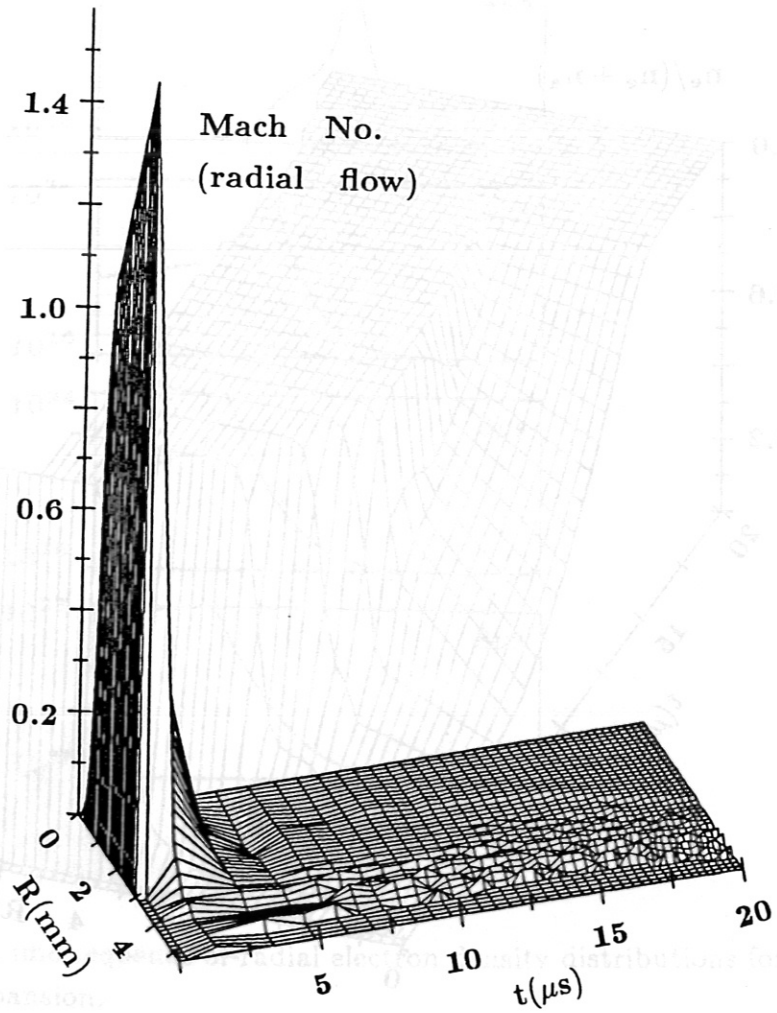

Figure 3: Time evolution of the radial distribution of the transverse flow Mach number during the mass addition phase.

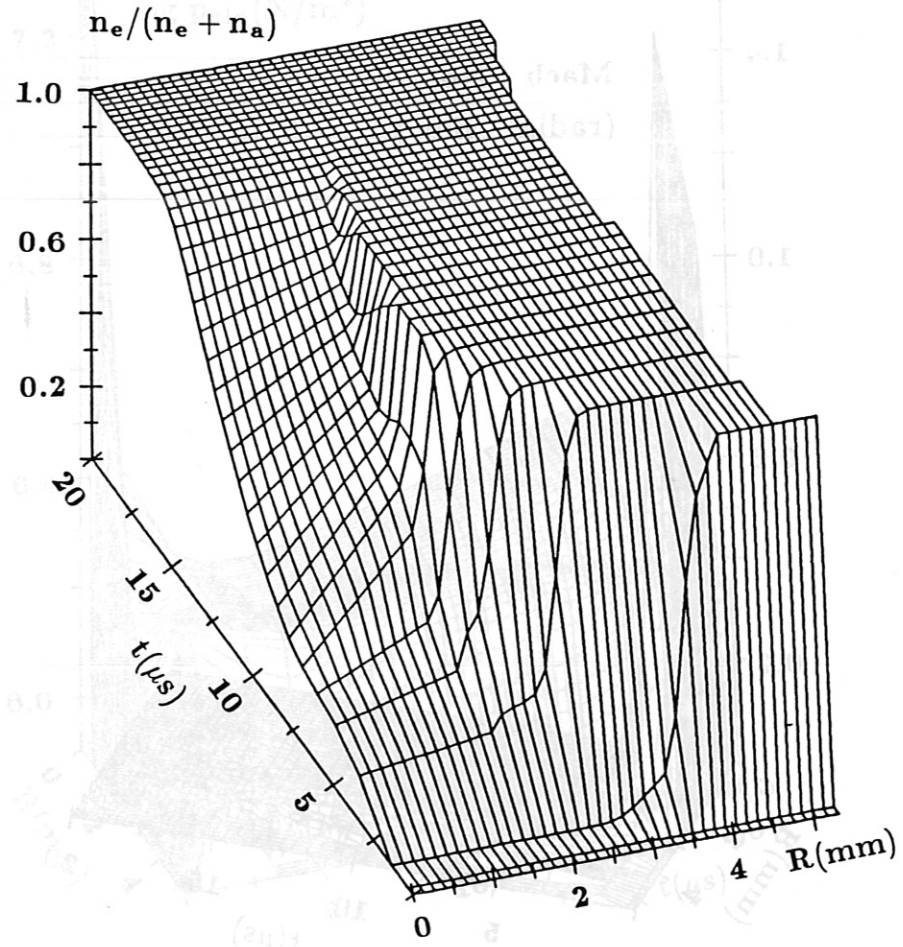

Figure 4: Time evolution of the radial ionization degree profile during the mass addition phase.

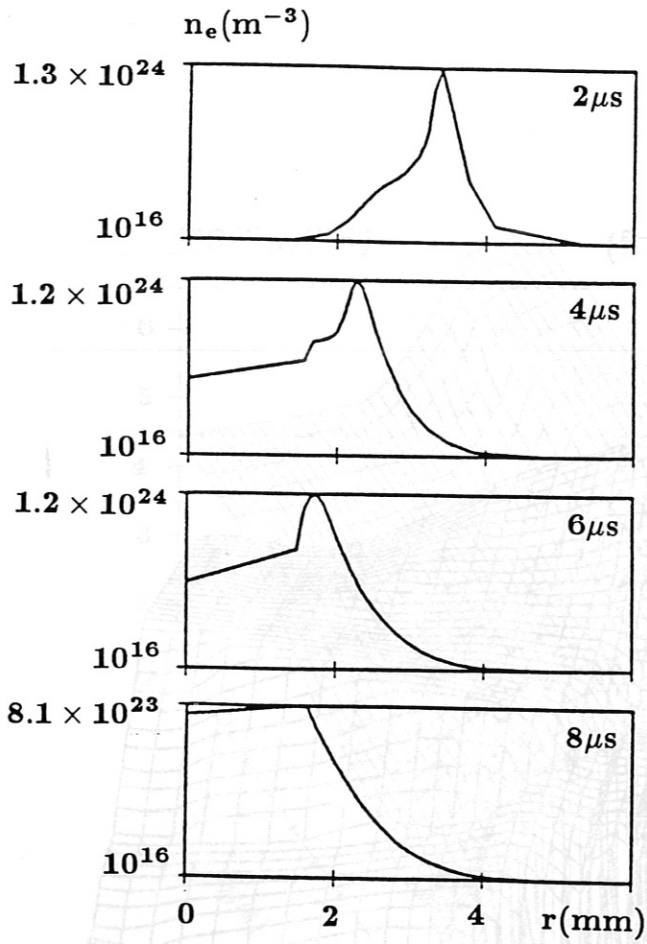

Figure 5: Time sequence of radial electron density distributions for the first 8 μs of the cloud expansion.

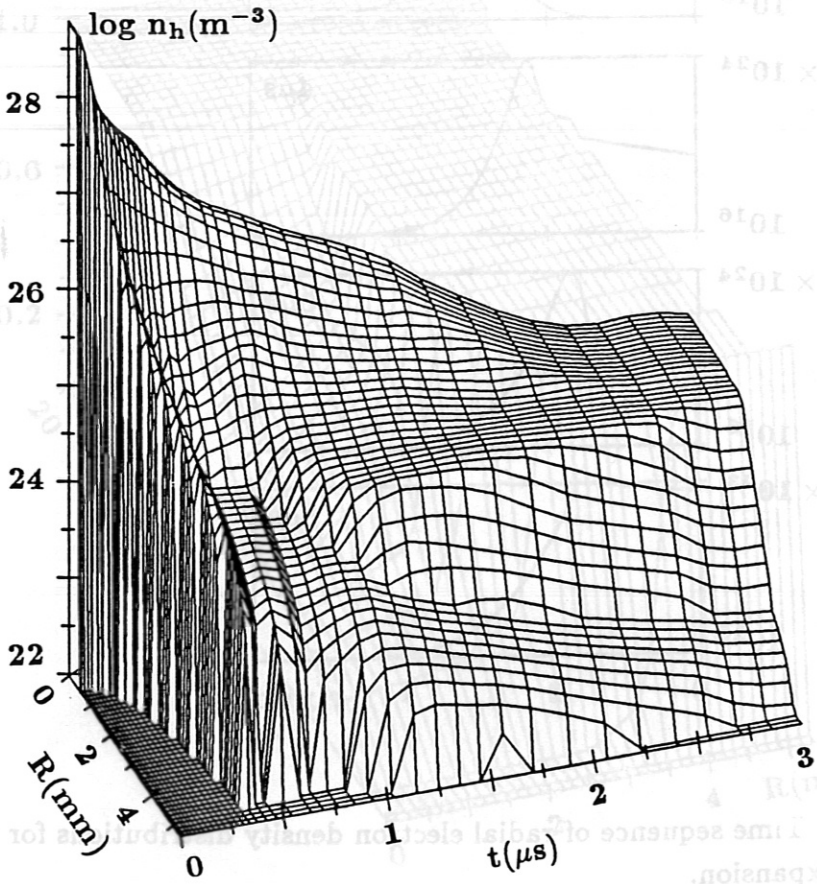

Figure 6: Time evolution of the heavy-particle density distribution during the first 3 μs of the cloud expansion.

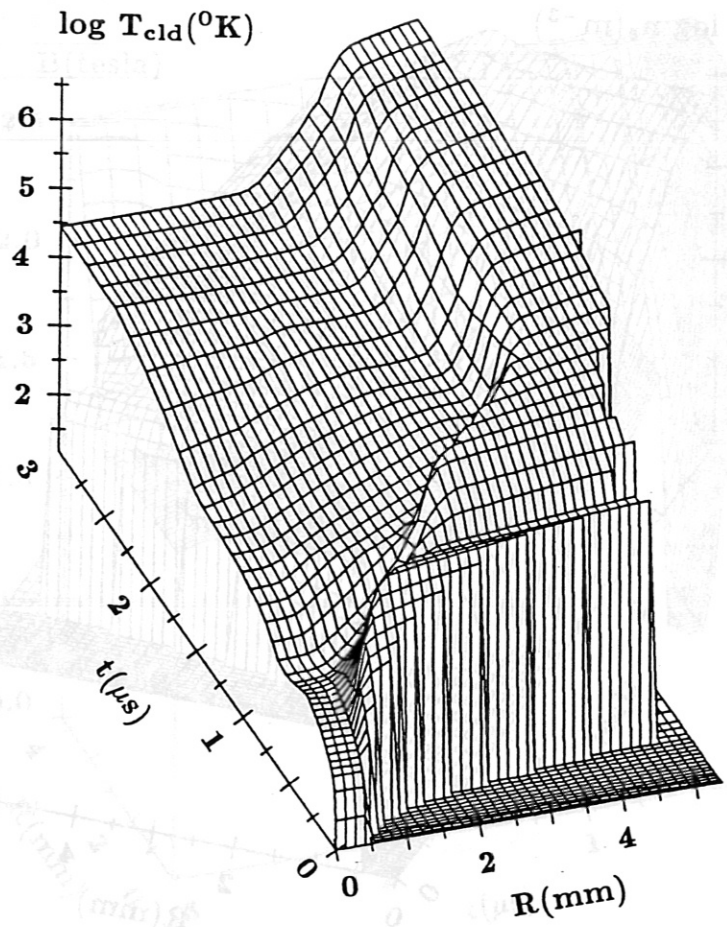

Figure 7: Time evolution of the temperature distribution during the first 3 μs of the cloud expansion (background plasma temperature is not displayed).

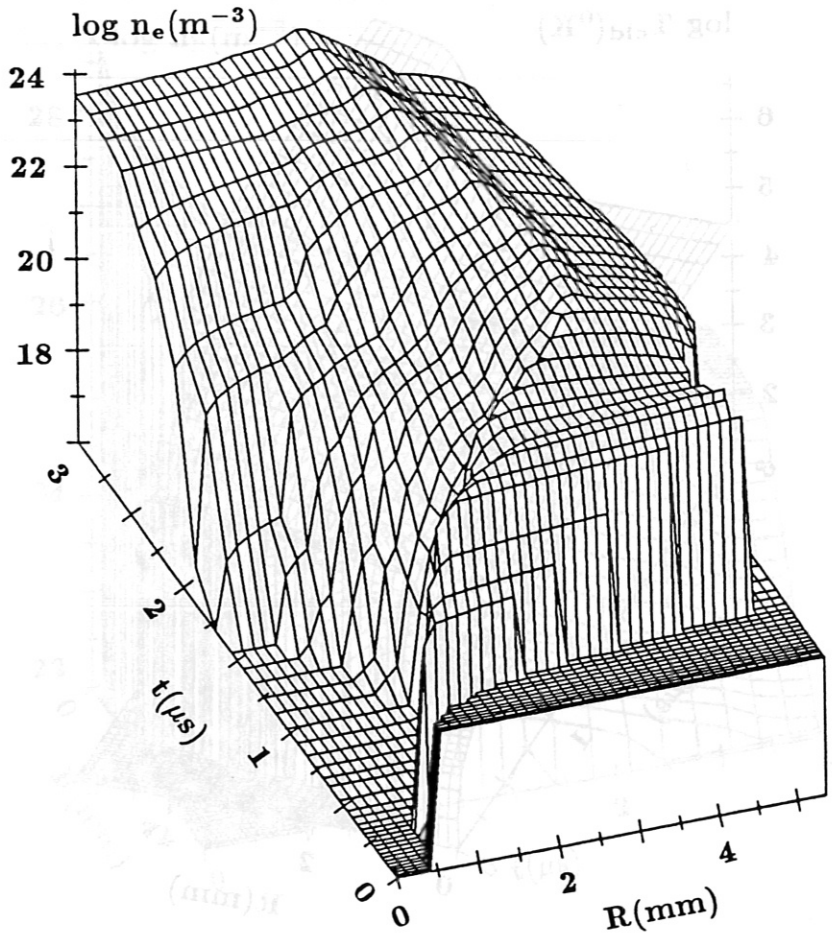

Figure 8: Time evolution of the electron density distribution during the first 3 μs of the cloud expansion.

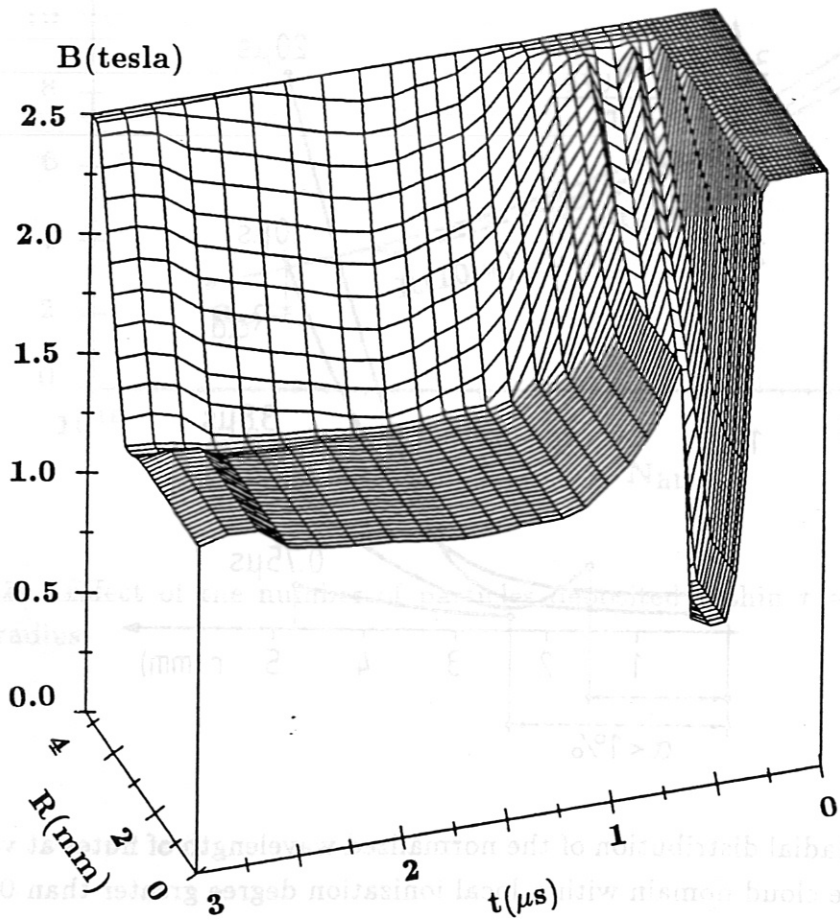

Figure 9: Time evolution of the magnetic field strength distribution during the first 3 μs of the cloud expansion.

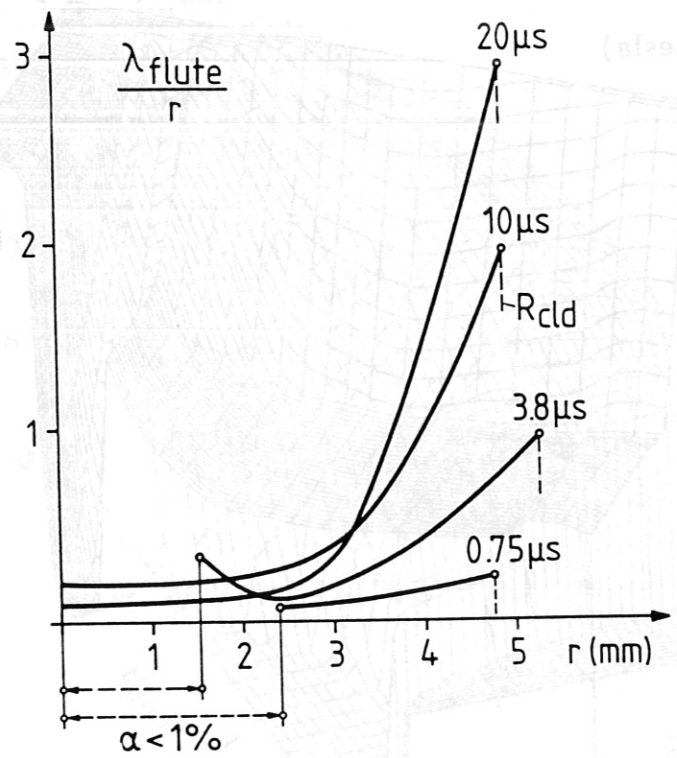

Figure 10: Radial distribution of the normalized wavelength of flutes at various time instants for the cloud domain with a local ionization degree greater than 0.01.

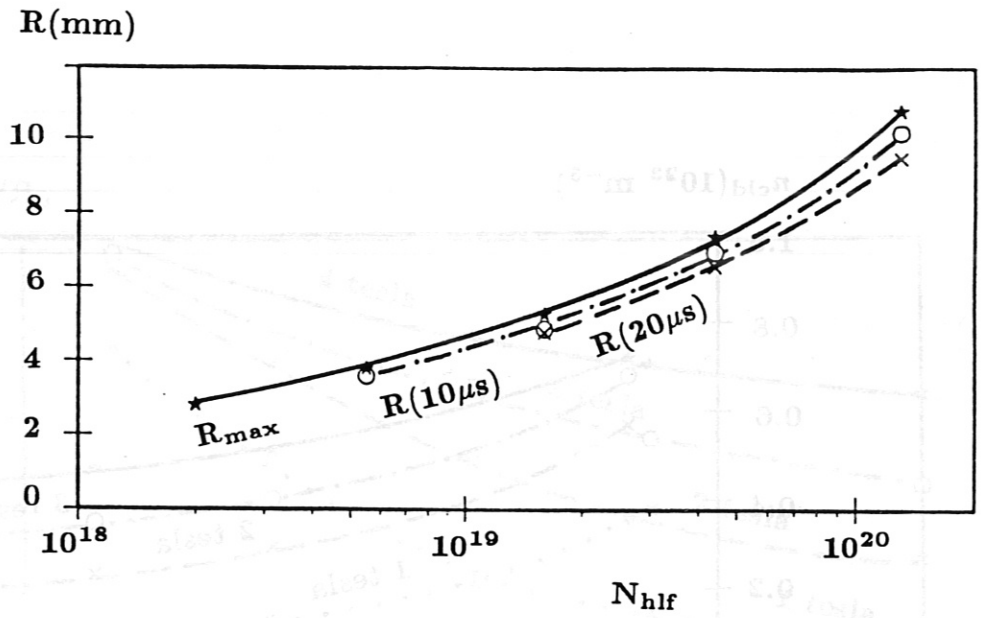

Figure 11: Effect of the number of particles deposited within $\tau = 20\ \mu s$ on the plasmoid radius.

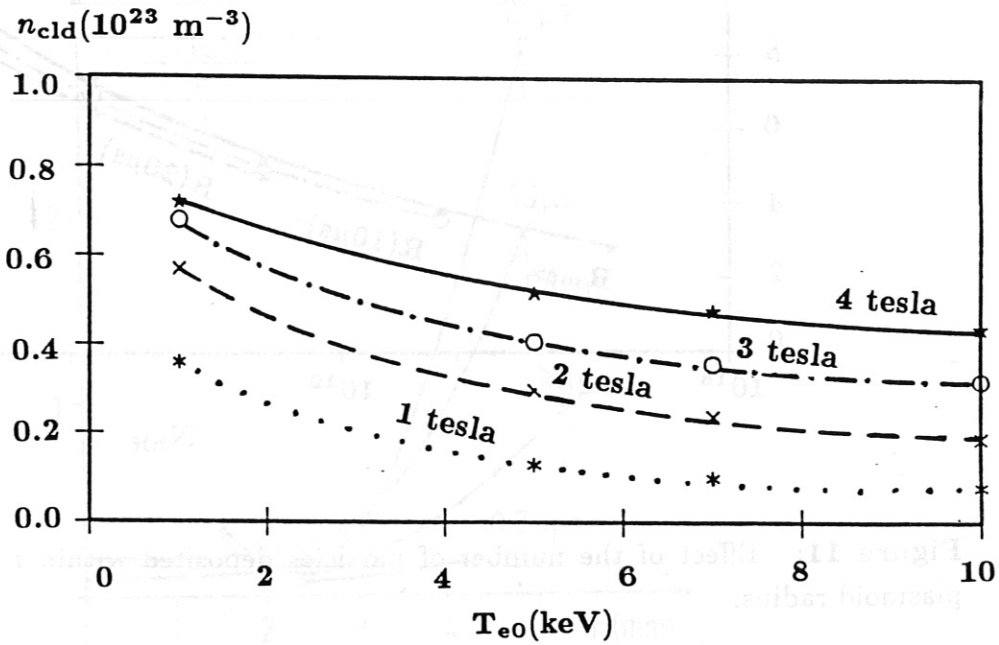

Figure 12: Cloud density after expansion time 20 μs as a function of plasma temperature and magnetic field strength.

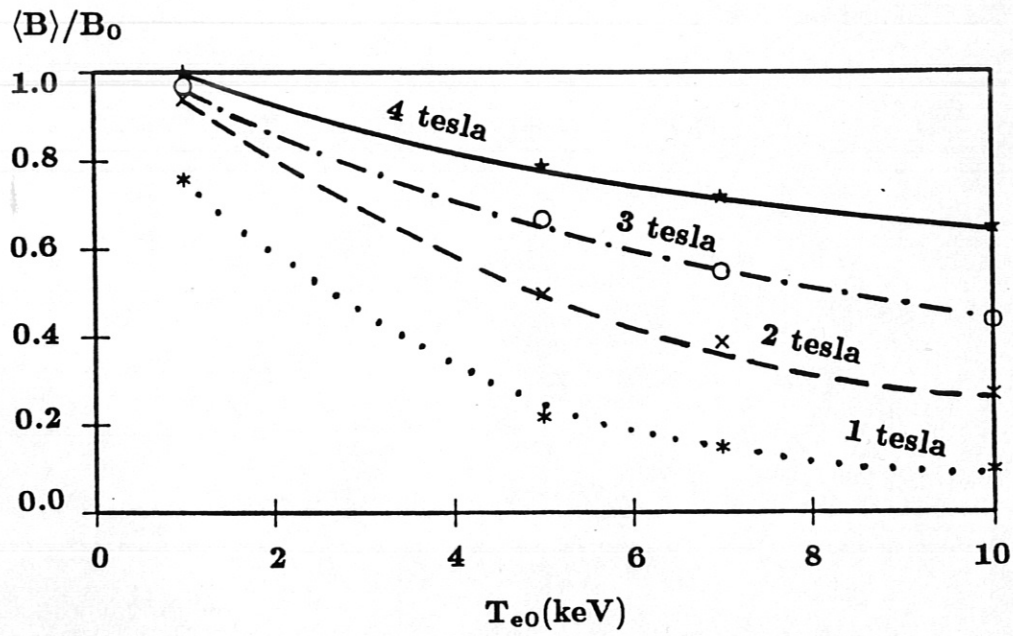

Figure 13: Diamagnetic state (average magnetic shielding factor) at $\tau = \tau(R_{max})$ as a function of plasma temperature and magnetic field strength.